Solar Phys (2017) 292:159
DOI 10.1007/s11207-017-1185-1

Non-neutralized Electric Currents in Solar Active Regions and Flare Productivity

Ioannis Kontogiannis[1] · Manolis K. Georgoulis[1] · Sung-Hong Park[2] · Jordan A. Guerra[2]

Received: 1 March 2017 / Accepted: 27 September 2017 / Published online: 19 October 2017

Abstract We explore the association of non-neutralized currents with solar flare occurrence in a sizable sample of observations, aiming to show the potential of such currents in solar flare prediction. We used the high-quality vector magnetograms that are regularly produced by the *Helioseismic Magnetic Imager,* and more specifically, the Space weather HMI Active Region Patches (SHARP). Through a newly established method that incorporates detailed error analysis, we calculated the non-neutralized currents contained in active regions (AR). Two predictors were produced, namely the total and the maximum unsigned non-neutralized current. Both were tested in AR time-series and a representative sample of point-in-time observations during the interval 2012 – 2016. The average values of non-neutralized currents in flaring active regions are higher by more than an order of magnitude than in non-flaring regions and correlate very well with the corresponding flare index. The temporal evolution of these parameters appears to be connected to physical processes, such as flux emergence and/or magnetic polarity inversion line formation, that are associated with increased solar flare activity. Using Bayesian inference of flaring probabilities, we show that the total unsigned non-neutralized current significantly outperforms the total unsigned magnetic flux and other well-established current-related predictors. It therefore shows good prospects for inclusion in an operational flare-forecasting service. We plan to use the new predictor in the framework of the FLARECAST project along with other highly performing predictors.

Keywords Active regions · Magnetic fields · Electric currents and current sheets · Flares · Forecasting

✉ I. Kontogiannis
jkonto@noa.gr

S.-H. Park
shpark@tcd.ie

[1] Research Center for Astronomy and Applied Mathematics (RCAAM), Academy of Athens, 4 Soranou Efesiou Street, Athens, 11527, Greece

[2] School of Physics, Trinity College Dublin, Dublin 2, Ireland

1. Introduction

Solar flares are localized and intense brightenings of the solar atmosphere, much brighter than the background, and they are evident throughout the entire electromagnetic spectrum. They are associated with *in situ* acceleration of energetic particles and (often) coronal mass ejections (CMEs), comprising some of the most spectacular and energetic phenomena of the solar system (Fletcher *et al.*, 2011). The overall associated energy, released in a very short time, is even exceeding 10^{32} erg in very large events that encompass both thermal and non-thermal processes.

The soft X-ray flux of a flare in the $1-8$ Å range, as recorded by the *Geostationary Operational Environmental Satellites* (GOES), is used to categorize solar flares in order from largest to smallest in a logarithmic scale of classes X, M, C, B, and A. These scales are complemented by decimal subclasses (M1.0, C5.2, *etc.*). Flares of M1.0 and higher are often referred to as major flares and affect the geospatial environment more than the others. On the other hand, B- and A-class flares are the weakest and often lie within the soft X-ray background produced by the global solar atmosphere.

Flares and CMEs affect the geospatial environment in diverse ways on timescales ranging from a few minutes to days. In flares, these effects are immediate. The electron density in a range of ionospheric altitudes is affected by the enhanced X-ray and EUV radiation, which disrupts radio communications, while the subsequent expansion of the atmosphere increases the drag on low-altitude satellites. Space-borne instrumentation and crew are also vulnerable to direct flare-related electromagnetic radiation and particles. This evident absence of early warning for flares and flare-related effects has necessitated the pursuit of accurate flare prediction. The scientific community has intensified efforts in this direction by incorporating the constant flow of solar magnetic observations that have been achieved during the past decades. This is done towards two complementary and often overlapping directions: on one hand, to understand the fundamental physics behind the flare phenomenon (Shibata and Magara, 2011), and on the other hand, to develop efficient flare prediction schemes (see *e.g.* Georgoulis, 2012b).

Energy released in flares is known to be stored in the intense, complex magnetic field configurations of solar active regions. The ability of magnetic fields to store energy is associated with their departure from a current-free (potential) state. This non-potentiality is evident in optical (Hα, Hβ), EUV, and X-ray images of the active region solar corona, where significant twist of the coronal loops is seen (Leka *et al.*, 1996; Schrijver, 2016). This twist requires substantial amounts of field-aligned electric currents. Therefore, the magnetic field configuration and the electric current distribution offer two aspects of the same physical reality (see *e.g.* Melrose, 1995, and references therein). Since inferring the electric currents requires the ability to record all three components of the magnetic field vector, studies focusing on electric currents and their role in flares started after vector magnetograms became widely available (see *e.g.* Canfield *et al.*, 1993; Zhang, 1995; Leka *et al.*, 1996, and references therein). Today, the regular flow of high temporal and spatial resolution photospheric vector magnetograms has boosted research in this topic (*e.g.* Ravindra *et al.*, 2011; Gosain, Démoulin, and López Fuentes, 2014; Janvier *et al.*, 2014; Vemareddy, Venkatakrishnan, and Karthikreddy, 2015; Inoue *et al.*, 2015).

A pertinent issue is whether electric currents in solar active regions are neutralized. In the ideal case of an isolated twisted flux tube embedded in a field-free medium, the net current along the tube should be zero, being equal to the sum of two opposite-directed currents: a direct (volume) current along its axis that produces its twist, and a return (surface) current that isolates the flux tubes from the field-free environment (Parker, 1979). Current neutralization subsequently means that direct and return currents balance each other within a given

magnetic polarity of an active region, giving rise to a zero net current *per* polarity. However, early calculations based on vector magnetograms showed that high values of net currents exist within active regions, implying a non-neutralization situation and a subsequent injection of net currents in the solar corona (Melrose, 1991, 1995).

Since then, a series of studies addressed the non-neutralization of photospheric electric currents and their origin. Most of them have shown that there are weak or no return currents in the photosphere (Leka *et al.*, 1996; McClymont, Jiao, and Mikic, 1997; Semel and Skumanich, 1998; Wheatland, 2000; Falconer, 2001), and it is now being largely accepted that the currents that run along the magnetic field lines are non-neutralized. However, there have been some opposing arguments, reporting the existence of return currents in isolated sunspots (Wilkinson, Emslie, and Gary, 1992). Moreover, according to Parker (1996), the observational limitations of magnetographs consequently lead to erroneous calculations of net electric currents with no physical meaning, when the differential form of Ampère's law is used.

To address the issues of spatial resolution and errors that may hinder the correct interpretation, Georgoulis, Titov, and Mikić (2012) proposed a detailed method for calculating the electric current neutralization. They also incorporated a detailed error analysis and imposed strict criteria on current neutralization. Their study of two active regions showed that intense non-neutralized currents are found exclusively at the vicinity of strong magnetic polarity inversion lines (MPIL) and that higher values are linked with higher flare productivity. Strong MPILs separate opposite polarities and are characterized by high magnetic field strength, leading to a plasma β on the order of unity at the photosphere. In such conditions, the Lorentz force can overcome the hydrodynamic inertia of the photospheric plasma and produce shear. It was therefore concluded that non-neutralized currents are injected in the atmosphere with the emergence of flux and that the shear observed in MPILs is generated by the Lorentz force when the cylindrical symmetry of the flux-tube footprints breaks down. Their results have not been reproduced since on a larger sample, but the exclusive relation between non-neutralized currents in MPILs and shearing/twisting motions has been demonstrated *via* observations and models in subsequent studies (Janvier *et al.*, 2014; Török *et al.*, 2014; Vemareddy, Venkatakrishnan, and Karthikreddy, 2015; Dalmasse *et al.*, 2015). Although there is no general consensus on the causal relationship between shearing motions and the Lorentz force, there seems to be a consensus that substantial net currents are injected in the corona along strong MPILs. Dissipative processes (magnetic reconnection) are required for current neutralization, justifying the use of current-related quantities as flare predictors.

Electric current densities have shown good correlation with flaring and coronal mass ejection (CME) activity (Falconer, Moore, and Gary, 2002; Yang *et al.*, 2012) and have been incorporated in flare prediction schemes in several studies (Leka and Barnes, 2003a,b, 2007; Bobra and Couvidat, 2015). In these studies, predictors related to the electric current rank among the best performing, motivating us to investigate new ones, based on the systematic approach of Georgoulis, Titov, and Mikić (2012), where the effects of numerical artefacts and magnetic field measurement errors are mitigated and the contribution of MPILs with strong shear, such as potential flaring sites in active regions, are intensified. Thus, we extend their results to a large sample of active regions, aiming to produce a new current-based predictor for use in the context of the FLARECAST project.

FLARECAST is a novel endeavor whose purpose is to produce real-time flare predictions of unmatched accuracy. It aims to do so by incorporating the most efficient predictors and methods in a highly sophisticated prediction scheme, exploiting advanced machine-learning techniques. Along with using the predictors proposed so far in the literature, part of the

Table 1 NOAA AR sample. $t_{\rm start}$ and $t_{\rm end}$ are the starting and ending dates of each time-series. The B, C, M, and X columns denote the number of flares in the corresponding flare class within this interval, FI is the corresponding flare index, while Mag.Type is the Mt.Wilson classification type of the NOAA AR.

NOAA AR	$t_{\rm start}$ (UT)	$t_{\rm end}$ (UT)	B	C	M	X	FI	Mag.Type
11072	2010-05-20 16:24	2010-05-24 22:36	2	0	0	0	0.06	β
11158	2011-02-10 21:59	2011-02-15 22:59	1	25	4	1	100.67	β–$\beta\gamma$
11429	2012-03-04 01:23	2012-03-10 22:35	0	34	12	6	278.15	$\beta\gamma$–$\beta\gamma\delta$
11515	2012-06-28 03:00	2012-07-07 19:48	2	39	14	0	53.97	β–$\beta\gamma\delta$
11640	2013-01-01 03:35	2013-01-05 22:59	5	4	0	0	1.81	β–$\beta\gamma\delta$
11663	2013-01-29 23:59	2013-02-03 22:23	2	2	0	0	0.55	β
11748	2013-05-15 02:36	2013-05-18 22:24	0	10	4	0	31.16	$\beta\gamma\delta$
11863	2013-10-10 02:35	2013-10-13 22:35	0	0	0	0	0.0	α–β
11875	2013-10-18 04:23	2013-10-28 10:23	0	81	18	2	93.60	β–$\beta\gamma\delta$
11882	2013-10-26 02:23	2013-10-30 22:35	0	7	10	0	49.10	$\beta\gamma\delta$–$\beta\gamma$
11923	2013-12-12 03:35	2013-12-15 22:35	0	0	0	0	0.0	β

project is devoted to developing new ones. In this context, we investigate the flare-prediction capability of the total and maximum non-neutralized electric currents in active regions. Our sample is statistically significant and consists of thousands of space-based active-region vector magnetograms acquired during the current Solar Cycle 24.

2. Dataset Description: SHARP Near Real-Time Data

We used observations from the *Helioseismic Magnetic Imager* (HMI; Scherrer *et al.*, 2012; Schou *et al.*, 2012) on board the *Solar Dynamics Observatory* mission (SDO; Pesnell, Thompson, and Chamberlin, 2012). Aiming to produce data that are specifically directed to space weather research, the HMI team have developed the Space weather HMI Active Region Patches (SHARP; Bobra *et al.*, 2014). These are cutouts that contain the magnetic field vector components, remapped and deprojected as if observed at the solar disk center along with a set of quantities used for predicting solar eruptions. In this study we used the near-real time (NRT) cylindrical equal area (CEA) SHARP data. Because we aim to use the non-neutralized currents as predictors in an automated flare-prediction service that will rely on the automatically produced HARP cutouts, no constraints on the solar disk location have been imposed in this study.

To initially test the algorithm and its performance and determine whether there is a correspondence between the evolution of the parameters and the flaring activity of active regions, a sample of 11 National Oceanic and Atmospheric Administration (NOAA) active regions (AR) was chosen. These ARs and the corresponding time-series durations, starts, and ends were selected randomly and show none, low, moderate, or high flare productivity. Table 1 summarizes the time-series start and end, the Mt.Wilson classification type, and the corresponding flare productivity of the active regions.

For further testing, a representative sample of SHARP cutouts was processed. We selected 336 random days between September 2012 and May 2016, which comprise 25% of the entire SHARP data coverage. For each day, we processed SHARP cutouts at a cadence of 6 h, resulting in 9454 data points.

The GOES[1] database was used to derive the flare association of the SHARP observations. For every HARP cutout of our sample (both active region time-series and the representative sample), we derived the flare onset times and classes within the following 24 h. Specifically for the time series, we also calculated the total flare index (FI) for the duration of each time-series, using the formula of Abramenko (2005), that is,

$$\mathrm{FI} = \left(100S^{(\mathrm{X})} + 10S^{(\mathrm{M})} + 1.0S^{(\mathrm{C})} + 0.1S^{(\mathrm{B})}\right)/\Delta t, \tag{1}$$

where $S^{(\mathrm{X,M,C,B})}$ is the *per* class sum of flare magnitude (the number that follows the class letter) and Δt is the time interval in days. The number of flares *per* class and the total flare index for the AR sample are shown in Columns 4 – 8 of Table 1. Of the 9454 points of the representative sample of SHARP CEA NRT cutouts, 2573, 212, and 16 are associated with C-, M-, and X-class flares, respectively, over the preset window.

3. Analysis: Non-neutralized Currents in Solar Active Regions

We followed the method of Georgoulis, Titov, and Mikić (2012), which incorporates measurement uncertainties and poses strict criteria on deciding whether the calculated currents are neutralized. Here we briefly describe the method, while we refer to the original article for more details.

The map of the radial component of the SHARP vector magnetic field is partitioned into non-overlapping patches of the same magnetic polarity, using a gradient-based flux tessellation scheme (Barnes, Longcope, and Leka, 2005). This partitioning method has also been used by Georgoulis and Rust (2007) for the calculation of the effective connected magnetic field strength. To ensure that quiet-Sun magnetic elements are excluded and only sizable AR-only magnetic polarities are taken into account, thresholds on magnetic field strength, enclosed magnetic flux, and area are imposed. According to Georgoulis, Titov, and Mikić (2012), small changes in the selected thresholds do not alter the essence of the results. Their conclusion was also verified in our dataset by testing thresholds, *e.g.* magnetic field strength up to 300 G and enclosed magnetic flux up to 10^{20} Mx. Using lower thresholds will result in more partitions, which will not contribute to the calculations but will dramatically slow up the process. The thresholds selected in magnetic field strength, enclosed magnetic flux, and size per partition are 100 G, 5×10^{19} Mx, and 40 pixel. Before partitioning, the input magnetograms were smoothed with a 5×5 pixel kernel to produce partitions with slightly smoother boundaries and (in the case of time-series) avoid dramatic changes of the partitioning process from frame to frame. The process returns all non-overlapping partitions, along with their flux-weighted centroid positions, boundaries, and corresponding magnetic fluxes.

For each partition, the vertical electric current density is calculated using the differential form of Ampère's law:

$$J_z = \frac{1}{\mu_0}\left(\frac{\partial B_y}{\partial x} - \frac{\partial Bx}{\partial y}\right), \tag{2}$$

where B_x and B_y are the two horizontal components of the magnetic field and μ_0 is the magnetic permeability of the vacuum. The total current I_i contained in each partition is calculated as the algebraic sum of the contained J_z. The error maps of the three components

[1] http://www.ngdc.noaa.gov/stp/satellite/goes/.

of the magnetic fields are used to calculate the corresponding error δI_i for each I_i. To decide whether I_i is non-neutralized, we calculated the corresponding potential magnetic field components (Alissandrakis, 1981) using the vertical magnetic field B_z as boundary condition and repeated the calculation for the potential magnetic field configuration. The value of current $I_i^{\rm pot}$ in this case should be, by definition, equal to zero. Owing to numerical effects, however, non-zero results are produced. The total electric current, I_i, of a given partition is considered non-neutralized, $I_i^{\rm NN}$, if it satisfies the following criteria: $I_i > 5 \times I_i^{\rm pot}$ and $I_i > 3 \times \delta I_i$. From the set of non-neutralized partition currents (if any) within the active region at a given time, we calculated the maximum value, $I_{\rm NN,max}$, and the total unsigned non-neutralized current $I_{\rm NN,tot}$. The latter is defined as the sum of the absolute current values of the non-neutralized partitions, $I_i^{\rm NN}$ *i.e.*,

$$I_{\rm NN,tot} = \sum_i \left| I_i^{\rm NN} \right|. \tag{3}$$

The rationale for selecting these two quantities is, as already mentioned, that strong flares in ARs are associated with MPILs, which are in turn associated with strong non-neutralized currents (Georgoulis, Titov, and Mikić, 2012; Dalmasse *et al.*, 2015; Vemareddy, Venkatakrishnan, and Karthikreddy, 2015). Several sites in an active region may develop suitable conditions for flaring. $I_{\rm NN,max}$ may be an indicator of the non-neutralized current that has increased at a certain site, while if several such locations are indeed present (hence $I_{\rm NN,tot}$ is increased), then the active region should be even more prone to strong flares.

It should be pointed out that our method ensures that the calculated parameters are not size dependent but exclusively linked to the presence of strong MPILs. In this sense, $I_{\rm NN,tot}$ and $I_{\rm NN,max}$ are not extensive but intensive, and therefore neither the size of an active region nor the extent of the cutout (so long as it fully contains the active region) affect the calculations.

We investigated the flare-predictive capability of $I_{\rm NN,max}$ and $I_{\rm NN,tot}$ in a twofold manner. First, we explored the time evolution of the non-neutralized currents of active regions in comparison with their flaring activity in order to assess whether the results of Georgoulis, Titov, and Mikić (2012) extend to more than the two cases the authors presented. Then, the performance of the two parameters was examined on a sizable sample of point-in-time observations that is representative of the sample that FLARECAST will rely on.

4. Results

4.1. General Trends, and Rationale for Using Non-neutralized Currents in the FLARECAST Project

The purpose of this section is to assess whether 1) more flare-productive ARs are linked with higher non-neutralized currents, 2) the two quantities show an evolution similar to their flare productivity, and 3) this evolution is suitable for prediction, *i.e.* if the increase in the two parameters precedes flares and shows some correlation with flare class or flare index within a given time-window.

In Figure 1 we plot the temporal evolution of the $I_{\rm NN,tot}$ and $I_{\rm NN,max}$ for each of the 11 active regions of the first sample. It is clear that flare-productive ARs have $I_{\rm NN,tot}$ and $I_{\rm NN,max}$ values that are higher by more than an order of magnitude. The strongest flares require the existence of systematically high non-neutralized currents such as in the case of

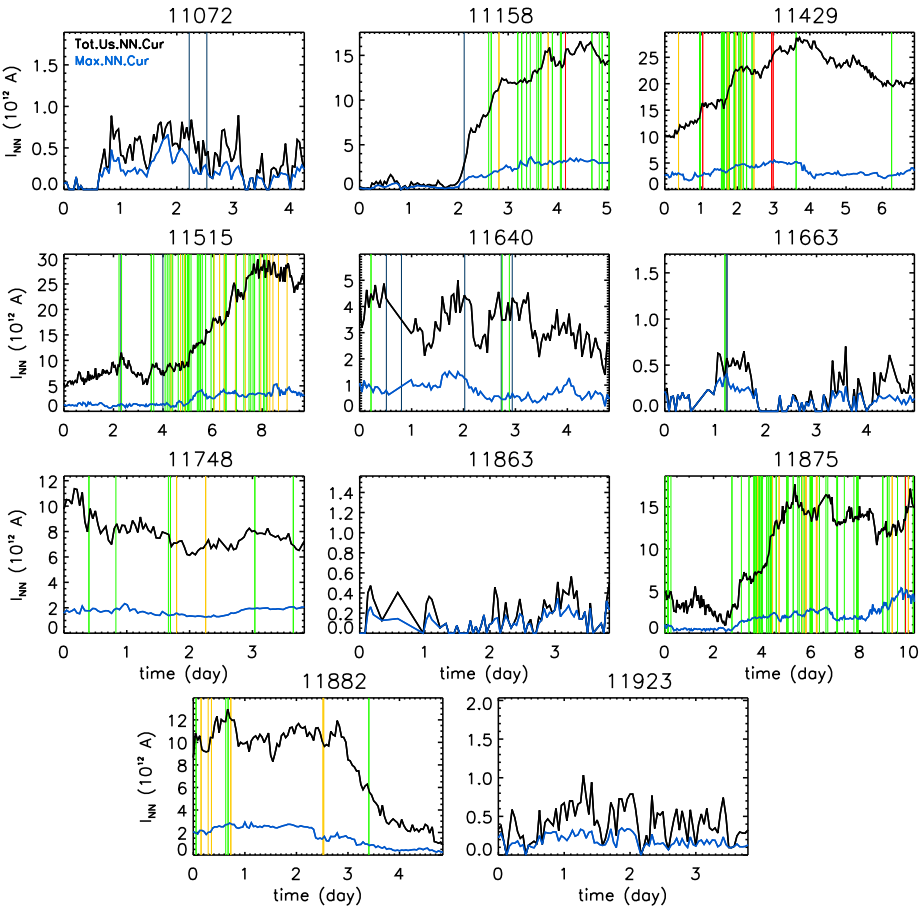

Figure 1 $I_{\mathrm{NN,tot}}$ (*black*) and $I_{\mathrm{NN,max}}$ (*blue*) temporal evolution of the 11 ARs of Table 1. *Blue, green, yellow,* and *red vertical lines* mark the start times of B-, C-, M-, and X-class flares.

ARs 11429, 11515, 11748, and 11875. Another interesting finding is that many strong flares are preceded by a few hours of increasing $I_{\mathrm{NN,tot}}$ (*e.g.* ARs 11158, 11515, and 11875). This increase corresponds to the emergence of new flux and to the development of a strong PIL and is also reflected on their magnetic type evolution (Table 1, last column).

Active regions with $I_{\mathrm{NN,tot}}$ and $I_{\mathrm{NN,max}}$ lower than 10^{12} A exhibit very low or no flaring activity at all. For instance, AR 11072 and AR 11663 produced only B or up to C1.1 class flares, respectively. In the latter case, these flares were clustered around relatively enhanced non-neutralized currents during the second day. This clustering of flares during well-defined peaks of $I_{\mathrm{NN,tot}}$ is also observed in AR 11640, which exhibits more frequent flaring activity, owing to its overall higher values of $I_{\mathrm{NN,tot}}$ and $I_{\mathrm{NN,max}}$.

To some extent, the more sizable flare-productive active regions also exhibit repeated flaring activity during peaks of the two parameters, although these peaks do not stand out clearly, but lie on an increased background because these active regions contain many non-neutralized partitions along intense MPIL, which increase the total amount of non-neutralized current. More careful inspection shows that even for these active regions, the

long temporal increase of non-neutralized currents exhibits structure on finer temporal scales, manifested by shorter peaks in addition to the general trend. This is seen mostly at the $I_{\mathrm{NN,tot}}$ curve, while the $I_{\mathrm{NN,max}}$ curve is less inclined. This difference may arise because the non-neutralized current of a given partition may not increase above a certain limit. Instead, the increasing number of non-neutralized partitions results in an overall increase of $I_{\mathrm{NN,tot}}$. We also note that intense flaring activity is found at times when $I_{\mathrm{NN,tot}}$ is several times higher than $I_{\mathrm{NN,max}}$. We return to this remark in the next section. By incorporating the added effect of multiple non-neutralized partitions within an active region, $I_{\mathrm{NN,tot}}$ seems to represent its evolution more efficiently, and in this sense, it may prove a more efficient flare predictor than $I_{\mathrm{NN,max}}$.

Accumulation of non-neutralized currents in AR partitions as part of an energy build-up process may be clearly seen in ARs 11158, 11429, 11515, and 11875. In AR 11158, the flux emergence that is observed at the end of the second day is accompanied by an increase in the total non-neutralized currents, showing that flux emergence results in the injection of net currents in the AR corona. This is in line with previous results on the origin of the non-neutralized currents. Georgoulis, Titov, and Mikić (2012) used a dimensionless non-neutralization factor to show that two active regions with very different flare productivity were coherent structures. This led the authors to conclude that the non-neutralized currents they contained had a sub-photospheric origin. Their results were corroborated by the magnetohydrodynamics (MHD) simulations of Török *et al.* (2014), which showed that active regions are born with substantial non-neutralized currents.

The association between non-neutralized current increase and flaring–CME activity has been implied in previous studies (see *e.g.* Ravindra *et al.*, 2011; Janvier *et al.*, 2014; Vemareddy, Venkatakrishnan, and Karthikreddy, 2015). In most of these studies, which prompt the evolution of an AR, this association was inferred *a posteriori* by manually selecting regions of interest, based on the sites of recorded flaring activity (around MPILs). Conversely, judging by Figure 1, it seems that the temporal variation of $I_{\mathrm{NN,tot}}$ and $I_{\mathrm{NN,max}}$ brings out the evolution of non-neutralized currents at the regions of interest as clear enhancements in addition to the overall evolution. During the strongest flares, the total non-neutralized current continues to increase, showing that the free energy build-up process continues and flares remove only a part of this energy. According to Janvier *et al.* (2014), a local increase of the current may be observed after the flare at the footpoints of the ribbons.

It has been shown that strong direct currents, with weak or no return currents (implying the existence of non-neutralized currents), are compatible with the existence of twisted flux ropes (Schrijver *et al.*, 2008). For instance, AR 11429 was one of the most flare-productive ARs of Cycle 24, whose total non-neutralized current content is the highest of the sample (along with that of AR 11515). AR 11429 exhibited strong MPIL, with strong shear, indicative of strong deviations from non-potentiality, justifying the build-up of large amounts of $I_{\mathrm{NN,tot}}$. It produced two X-class flares at the end of day 3, both accompanied by CMEs, which were preceded by the formation of magnetic flux ropes (Chintzoglou, Patsourakos, and Vourlidas, 2015; Syntelis *et al.*, 2016). The X-class flare of the well-studied AR 11158 has also been associated with a flux rope formation (Inoue *et al.*, 2015). These comparisons are useful as they possibly link the proposed predictors with the underlying physics of the flaring phenomenon. A more detailed examination exceeds the scope of the present study and will be reserved for the future.

From a flare-forecasting point of view, we may infer approximate $I_{\mathrm{NN,tot}}$ thresholds of 0.5×10^{12}, 5×10^{12}, and 15×10^{12} A for C-, M-, and X-class flares to occur. However, except for one case where a C-class flare occurred for 0.5×10^{12} A (AR 11663), for the rest of the sample, a $I_{\mathrm{NN,tot}}$ value of at least 3×10^{12} A was observed. Of course these thresholds

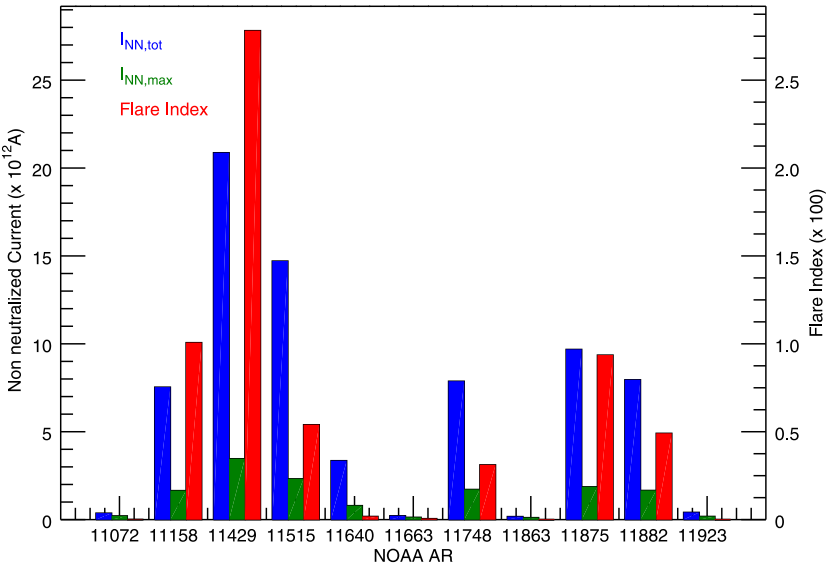

Figure 2 Time-averaged $I_{\mathrm{NN,tot}}$ (*blue*) and $I_{\mathrm{NN,max}}$ (*green*) for each active region of Table 1 and the corresponding flare index (*red*), calculated for the entire duration of each time-series of Figure 1.

are indicative: the actual merit of $I_{\mathrm{NN,tot}}$ and $I_{\mathrm{NN,max}}$ is examined in the next section. Still, the good correspondence between $I_{\mathrm{NN,tot}}$, $I_{\mathrm{NN,max}}$ and flare productivity is also illustrated in Figure 2. There, we plot the flare index during the observation interval for each AR of Figure 1 along with the corresponding temporal averages of the two examined predictors. From this plot it is also confirmed that quiet and flare-productive ARs differ by more than an order of magnitude in terms of non-neutralized current content. The Pearson correlation coefficients between FI and $I_{\mathrm{NN,tot}}$, $I_{\mathrm{NN,max}}$ are 0.869631 and 0.865931, respectively. We therefore conclude that the flare productivity of active regions is very well correlated with their amount of non-neutralized electric currents.

4.2. $I_{\mathrm{NN,tot}}$ and $I_{\mathrm{NN,max}}$ as Solar Flare Predictors

Manually selected active region samples are useful to (visually) assess whether there is flare-predictive potential in certain active region properties, in order to test the performance of the calculation algorithms, and to fine-tune the input parameters. The time evolution of these properties also often allows deriving some association with the physical processes that are involved in the flaring phenomenon. Nevertheless, these samples, however randomly selected, are inherently different than the samples that are actually used in automated prediction services, where photospheric magnetogram cutouts are produced in real time and no (human-biased) selection effects apply. To accommodate an examination of $I_{\mathrm{NN,tot}}$ and $I_{\mathrm{NN,max}}$ in "realistic" conditions, we used the representative sample of 9454 SHARP CEA NRT vector magnetograms.

The corresponding non-zero $I_{\mathrm{NN,tot}}$ and $I_{\mathrm{NN,max}}$ are presented as a scatter plot in Figure 3 along with color-coded flare association information. It is clearly seen that most cutouts that are associated with major flares within the next 24 h (marked with yellow and red crosses) are found towards the upper right corner, *i.e.* are associated with higher non-neutralized electrical currents. It therefore seems that the two parameters allow a partial separation between

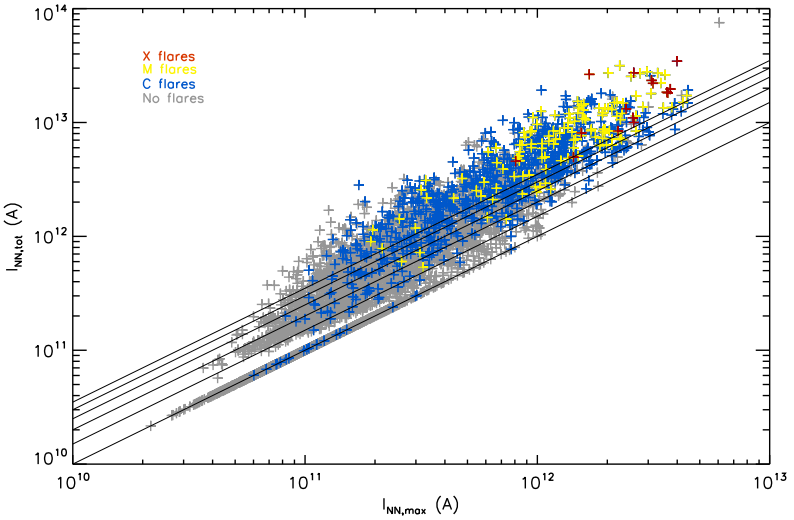

Figure 3 $I_{\mathrm{NN,tot}}$ *vs.* $I_{\mathrm{NN,max}}$ for the representative sample of SHARP CEA NRT cutouts with non-zero non-neutralized currents. Lower to upper *diagonal lines* mark the $I_{\mathrm{NN,tot}} = [1, 1.5, 2, 2.5, 3, 3.5] \cdot I_{\mathrm{NN,max}}$ fits.

flaring and non-flaring regions. For major flares to occur within the following 24 h, approximate thresholds of $I_{\mathrm{NN,tot}}$ and $I_{\mathrm{NN,max}}$ may be derived: 5×10^{11} A ($I_{\mathrm{NN,tot}}$) and 1.9×10^{11} A ($I_{\mathrm{NN,max}}$) for M-class flares and 4.6×10^{12} A ($I_{\mathrm{NN,tot}}$) and 8×10^{11} A ($I_{\mathrm{NN,max}}$) for X-class flares.

From the examination of the time evolution of the parameters in the previous section (Figure 1), we found that intense flaring occurs at times when the difference between $I_{\mathrm{NN,tot}}$ and $I_{\mathrm{NN,max}}$ is largest, while in quiet phases, the two quantities are roughly equal (or both close to zero). Figure 3 allows us to extend these results to a larger sample. It can be seen that no major flares are found below the $I_{\mathrm{NN,tot}} = I_{\mathrm{NN,max}}$ line: M- and X-class flares require $I_{\mathrm{NN,tot}} > 1.5 \cdot I_{\mathrm{NN,max}}$ and $I_{\mathrm{NN,tot}} > 3.5 \cdot I_{\mathrm{NN,max}}$, respectively. Therefore, major flares require the presence of many non-neutralized partitions. A large number of non-neutralized partitions denotes the presence of a stronger, more fragmented MPIL. It is well established that strong complicated MPILs are linked with high non-potentiality of the magnetic field (*e.g.* Falconer, Moore, and Gary, 2002; Schrijver, 2007) and strong shear and that they are consequently related to major flares. It is reasonable to suggest that if an AR contains several MPILs or one extended/more complicated MPIL, it is more prone to flare. While it seems that one single partition may reach a specific amount of non-neutralized current (reflecting high $I_{\mathrm{NN,max}}$), the presence of many non-neutralized partitions (either because there are several non-neutralized partitions along an MPIL or because there are several MPILs within an AR) results in $I_{\mathrm{NN,tot}}$ being several times higher than $I_{\mathrm{NN,max}}$. The findings of Figure 3 are therefore an alternative way to demonstrate that strong, fragmented MPILs are required for major flares and that this requirement is effectively incorporated in the definition of $I_{\mathrm{NN,tot}}$.

Next, we compared the performance of $I_{\mathrm{NN,tot}}$ and $I_{\mathrm{NN,max}}$ with that of the total unsigned flux, Φ_{tot}, and the two electric current-related parameters given by the SHARP team, that is, the total vertical current $J_{z,\mathrm{tot}}$ and the sum of the modulus of the average net current *per* polarity $J_{z,\mathrm{sum}}$ (Bobra *et al.*, 2014). The two latter parameters express the amount of net current in an active region, and the aim of the comparison is to investigate in practice whether $I_{\mathrm{NN,tot}}$ and $I_{\mathrm{NN,max}}$ have meaningful or trivial differences with these already established parameters.

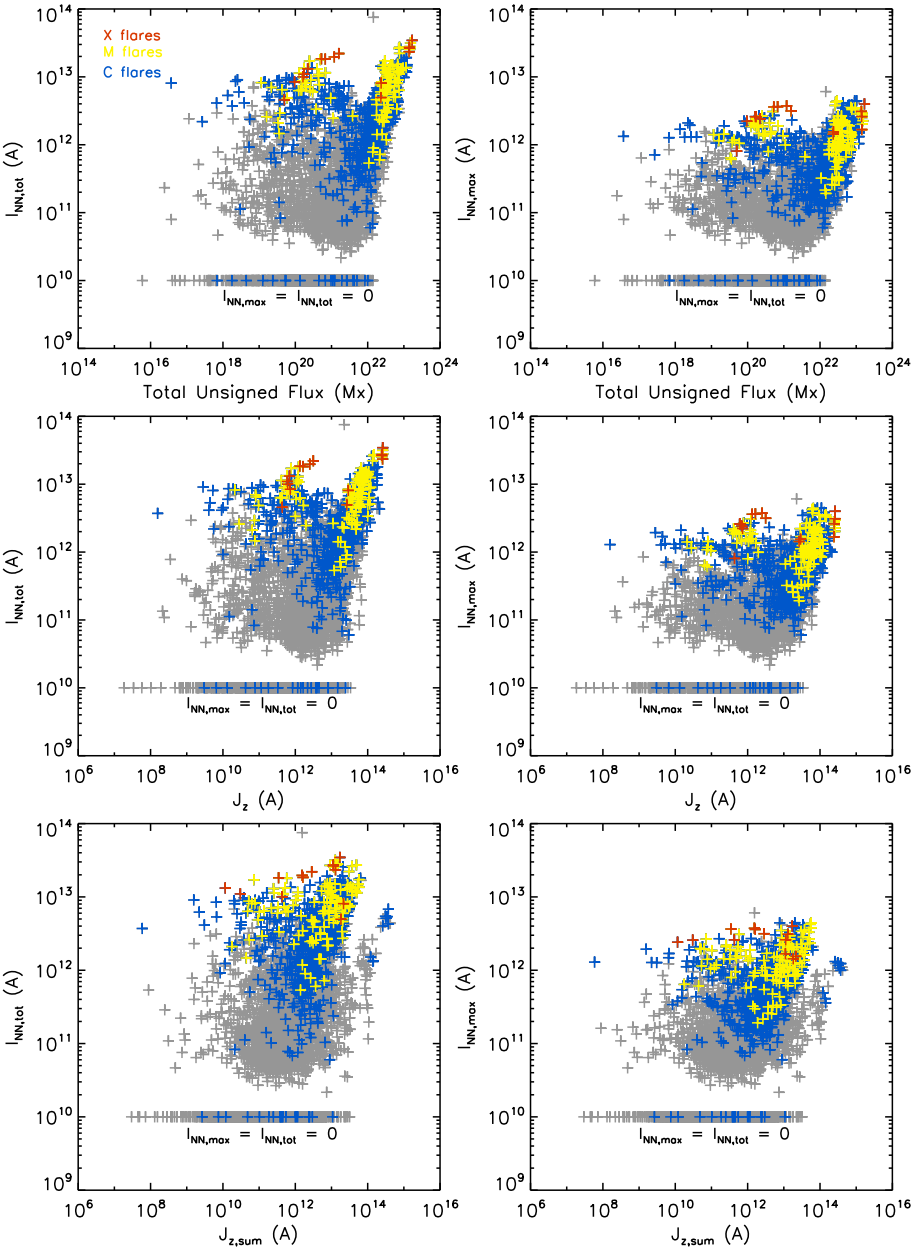

Figure 4 $I_{\mathrm{NN,tot}}$ (*left*) and $I_{\mathrm{NN,max}}$ (*right*) *vs.* Φ_{tot} (*top*), the total unsigned vertical current J_z (*middle*) and the sum of the modulus of the average net current *per* polarity $J_{z,\mathrm{sum}}$(*bottom*). The points associated with flares within 24 h are noted in different colors.

The scatter plots between parameters calculated for each of the 9454 points are found in Figure 4. Cutouts associated with flares of different classes that occur over the next 24 hours are denoted differently. The calculation process produced zero or no results for many cases.

This is either because some cutouts contained no non-neutralized partitions or because the partitioning process was, at times, unable to provide eligible partitions as *per* the preset thresholds. Both cases may include decaying or developing AR without MPILs and were treated as corresponding to zero $I_{\mathrm{NN,tot}}$ and $I_{\mathrm{NN,max}}$. These points are included in all panels of Figure 4 at an ordinate equal to 10^{10} A.

In general, all panels in Figure 4 imply at best a weak correlation between the examined parameters. The highest values of Φ_{tot} and J_z correlate better with $I_{\mathrm{NN,tot}}$ and $I_{\mathrm{NN,max}}$. These points also correspond to increased flaring activity, as most of the major flares (yellow and red crosses) are concentrated there.

It is also obvious that zero non-neutralized electric currents do not correspond to zero Φ_{tot}, J_z, and $J_{z,\mathrm{sum}}$. These are, by definition, extensive parameters, *i.e.* they increase with the size of the active region and/or the extent of the cutout and acquire non-zero values. On the other hand, $I_{\mathrm{NN,tot}}$ and $I_{\mathrm{NN,max}}$ are intensive (non-extensive) parameters, as they depend only on the size and strength of the MPIL and are zero when no MPILs are formed, regardless of the cutout extent. In our sample we find that only a very small fraction of these cutouts ($\sim 0.5\%$) are associated with C-class flares and none with M- or X-class flares.

The qualitative characteristics of the scatter plots of Figure 4 are quantified in terms of flare-forecasting potential by the Bayesian-inferred probabilities (Georgoulis, 2012a; Wheatland, 2005) in Figure 5. For a given threshold, normalized to the maximum value of each parameter to facilitate comparison, we count the total number, N, of active regions with a parameter value higher than the threshold and the number, F, of them that are flaring within the next 24 h. Then, the Bayesian probability is given by

$$p = \frac{\mathrm{F}+1}{\mathrm{N}+2}, \tag{4}$$

with an uncertainty of

$$\delta p = \sqrt{\frac{p(1-p)}{\mathrm{N}+3}}. \tag{5}$$

The calculated Bayesian probabilities of the five parameters as functions of the normalized thresholds are shown in Figure 5. The two non-neutralized current parameters produce more significant probabilities than Φ_{tot}, J_z, and $J_{z,\mathrm{sum}}$ for a range of normalized thresholds. As expected, $I_{\mathrm{NN,tot}}$ is more efficient. For C-class flares and flares higher than C-class, the difference with Φ_{tot} starts at $\sim$0.1 for low thresholds and exceeds 0.4. For major solar flares, the performance of $I_{\mathrm{NN,tot}}$ is significantly better than the Φ_{tot}. It should be noted that for very high thresholds the uncertainties increase, as the number of eligible data points (N) becomes smaller, which decreases the significance of the statistical sample. The results of Figure 5 suggest that $I_{\mathrm{NN,tot}}$ and $I_{\mathrm{NN,max}}$ are more efficient than Φ_{tot}, J_z, and $J_{z,\mathrm{sum}}$ at separating flaring from non-flaring active regions. They are therefore worth considering as flare predictors.

5. Discussion and Conclusions

In the context of an operational flare-forecasting service, we processed a sizable sample of SDO/HMI SHARP cutouts, aiming to examine the forecasting potential of two predictors related to the amount of non-neutralized electric currents contained in active regions. For the first time, we studied the evolution of the total and maximum unsigned non-

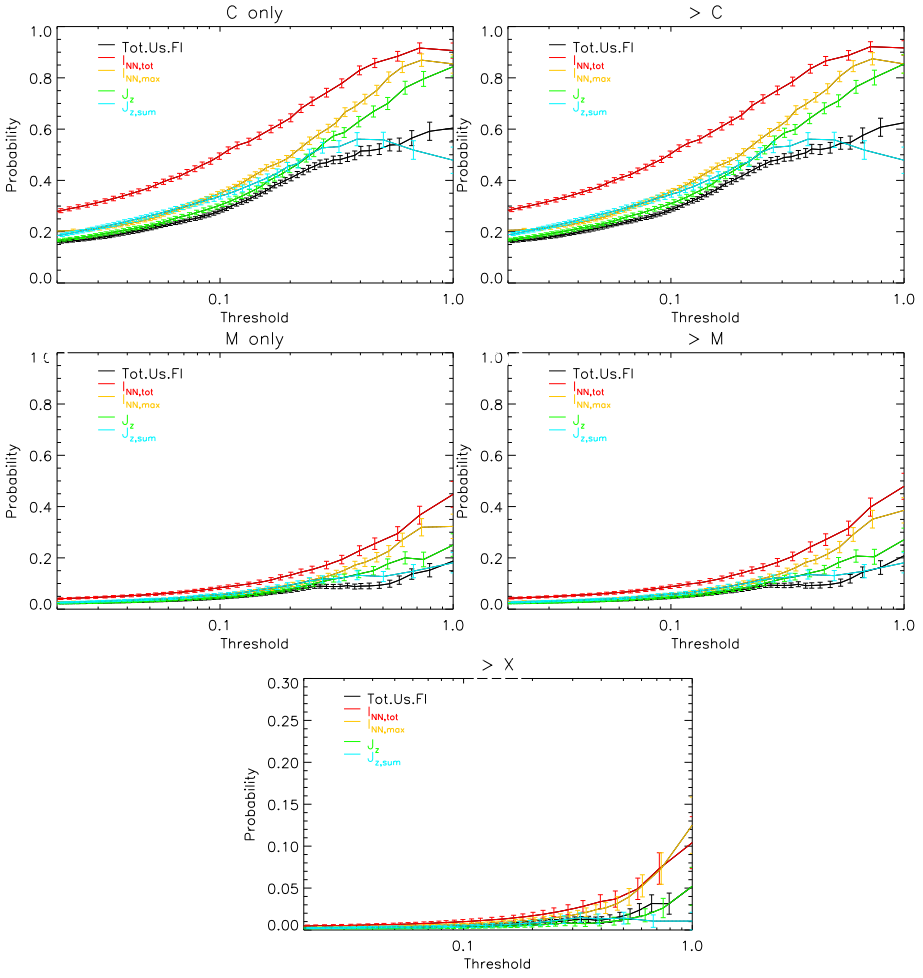

Figure 5 Bayesian-inferred probabilities of $I_{\mathrm{NN,tot}}$ (*red*) and $I_{\mathrm{NN,max}}$ (*orange*) compared with those of Φ_{tot} (*black*), J_z (*green*), and $J_{z,\mathrm{sum}}$ (*cyan*) for C-, M-, X-, above C-, and above M-class flares. Φ_{tot}, J_z, $J_{z,\mathrm{sum}}$, $I_{\mathrm{NN,tot}}$, and $I_{\mathrm{NN,max}}$ thresholds have been normalized to the corresponding maximum values, *i.e.* 1.68917×10^{23} Mx, 2.59441×10^{14} A, 4.21399×10^{13} A, 7.52898×10^{13} A, and 6.06393×10^{12} A, respectively. Each bin has the same statistical weight to facilitate comparison.

neutralized currents, $I_{\mathrm{NN,tot}}$ and $I_{\mathrm{NN,max}}$, for 11 active regions, as well as their performance in flare prediction in a representative sample of SHARP CEA NRT data, consisting of 9454 cutouts.

A brief discussion of the temporal evolution of these two new parameters showed that they correspond to physical processes such as MPIL formation, and as *per* previous studies, to a possible flux rope formation, closely related with intense flaring activity. After focusing on the potential of the $I_{\mathrm{NN,tot}}$ and $I_{\mathrm{NN,max}}$ as solar flare predictors, however, we did not discuss the origin and evolution of non-neutralized currents in active regions thoroughly. This is a long-standing question that has been addressed through simulations and observations (Georgoulis, 2017), and a more detailed investigation is pending.

Both parameters are closely associated with flare productivity, confirming and extending the conclusions drawn by Georgoulis, Titov, and Mikić (2012). It was shown for the first time, using a large representative sample of Solar Cycle 24, that both predictors are worth considering in automated flare prediction schemes. Of the two proposed predictors, $I_{\mathrm{NN,tot}}$ characterizes the flaring potential of an active region more efficiently because it encompasses the contributions of all possible flare-producing sites within an active region.

An important advantage of these predictors is that they include a detailed error analysis in the calculations of the non-neutralized currents. This approach has proven to be reliable for concluding whether the currents in ARs are neutralized (Georgoulis, Titov, and Mikić, 2012). The immediate comparison with the potential field ensures that the measured currents do exist and are significant through existing observations and are not due to the numerical effects that arise when analytical expressions (such as Ampère's law) are applied to discretized distributions of continuous physical quantities (such as the magnetic flux density). Therefore, possibly erroneous electric currents are constrained. Qualitatively, our results also suggest that the method we used does not depend on the resolution of the processed magnetograms. The method was originally developed for *Hinode* SOT/SP magnetograms, which have the highest resolution available to date, and in this study was applied to the lower resolution SDO/HMI vector magnetograms. For all the reasons mentioned, $I_{\mathrm{NN,tot}}$ is more advantageous than other commonly used current parameters, such as the total vertical current density, J_z, or the total unsigned current *per* polarity.

This said, the association between $I_{\mathrm{NN,tot}}$ and J_z is not trivial since by definition, there is no linear relationship between the two predictors. The total unsigned current of an active region is an extensive parameter, meaning that in principle, it increases with the size of the active region (similarly to Φ_{tot}). Non-neutralized currents, on the other hand, should be zero for active regions that do not contain strong MPILs or for SHARP cutouts that lack one polarity, regardless of their magnetic flux content and vertical electric current density. Therefore, $I_{\mathrm{NN,tot}}$ and $I_{\mathrm{NN,max}}$ are non-extensive parameters (as the lack of correlation in Figure 4 also demonstrates), which incorporate in a physical way morphological information in active regions with possible (and plausible) implications for flare triggering (*i.e.* strong and sheared MPILs). Given that current-related parameters have shown good prospects for flare prediction (Bobra and Couvidat, 2015), we expect improved results for $I_{\mathrm{NN,tot}}$. In addition, non-extensive parameters were found to outperform the extensive ones in CME prediction (Bobra and Ilonidis, 2016), which means that there may be some potential in extending the usage of $I_{\mathrm{NN,tot}}$ to CME prediction as well.

In view of numerous studies on solar flare prediction, it has now become apparent that no single flare-predictor suffices to categorically forecast solar flares and that active regions are complex dynamical systems where more than one parameter is involved in flare triggering. Investigating the evolution and absolute magnitudes of non-neutralized electric currents is more attractive and tractable in the era of systematically and regularly available vector magnetograms. It is thus tempting to explore the possibility of producing, in the future, several predictors that involve such currents. For the moment, we are planning to include $I_{\mathrm{NN,tot}}$ in the set of predictors that will feed machine-learning algorithms in the framework of the FLARECAST project, at the same time investigating their physical significance *via* the project's explorative research component.

Acknowledgements We would like to thank the anonymous referee for constructive comments on the manuscript. This research has been funded by the European Union's Horizon 2020 research and innovation programme Flare Likelihood And Region Eruption foreCASTing (FLARECAST) project, under grant agreement No. 640216. The data used are courtesy of NASA/SDO, the HMI science team, and the Geostationary Satellite System (GOES) team. This work also used data provided by the MEDOC data and operations center (CNES/CNRS/Univ. Paris-Sud), http://medoc.ias.u-psud.fr/.

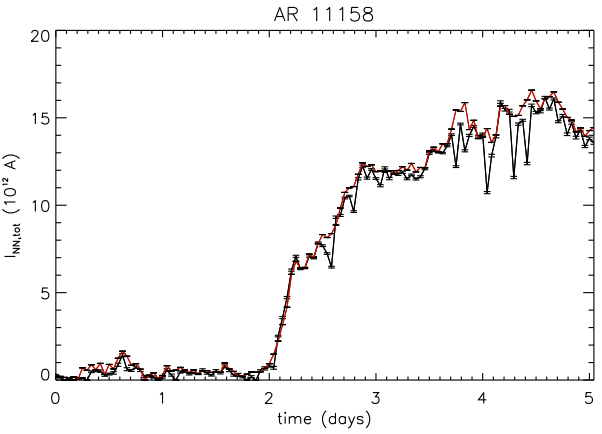

Figure 6 Total non-neutralized current, $I_{NN,tot}$ of AR 11158 as a function of time, calculated using the integral (*black*) and differential (*red*) form of Ampère's law.

Disclosure of Potential Conflicts of Interest The authors declare that they have no conflicts of interest.

Appendix: Differential *Versus* Integral Form of Ampère's Law

In the original work of Georgoulis, Titov, and Mikić (2012), the integral form of Ampère's law was chosen as being more accurate, although more time consuming. To examine the trade-off between speed and accuracy, we used both versions to calculate the total unsigned non-neutralized current for AR 11158. The results are shown in Figure 6, which shows that the two versions produce practically the same results. For the longer part of the time series, currents calculated by the two versions are the same within the uncertainties. For most of the points, the differences are within the error bars, and the two curves differ only at a few points. Overall, the differential form of Ampère's law produces slightly smoother curves, since it uses a larger number of pixels, which smoothes out differences from image to image (which could be due to noise or errors in the azimuth disambiguation and deprojection). Because it is based on the definition of a "correct" contour around each partition, the integral form is more sensitive to these variations. In view of this result and because the integral form of Ampère's law is significantly more time consuming, we chose to use the differential form to calculate the electric currents that correspond to each partition.

References

Abramenko, V.I.: 2005, Relationship between magnetic power spectrum and flare productivity in solar active regions. *Astrophys. J.* **629**, 1141. DOI. ADS.

Alissandrakis, C.E.: 1981, On the computation of constant alpha force-free magnetic field. *Astron. Astrophys.* **100**, 197. ADS.

Barnes, G., Longcope, D.W., Leka, K.D.: 2005, Implementing a magnetic charge topology model for solar active regions. *Astrophys. J.* **629**, 561. DOI. ADS.

Bobra, M.G., Couvidat, S.: 2015, Solar flare prediction using SDO/HMI vector magnetic field data with a machine-learning algorithm. *Astrophys. J.* **798**, 135. DOI. ADS.

Bobra, M.G., Ilonidis, S.: 2016, Predicting coronal mass ejections using machine learning methods. *Astrophys. J.* **821**, 127. DOI. ADS.

Bobra, M.G., Sun, X., Hoeksema, J.T., Turmon, M., Liu, Y., Hayashi, K., Barnes, G., Leka, K.D.: 2014, The Helioseismic and Magnetic Imager (HMI) vector magnetic field pipeline: SHARPs – space-weather HMI active region patches. *Solar Phys.* **289**, 3549. DOI. ADS.

Canfield, R.C., de La Beaujardiere, J.-F., Fan, Y., Leka, K.D., McClymont, A.N., Metcalf, T.R., Mickey, D.L., Wuelser, J.-P., Lites, B.W.: 1993, The morphology of flare phenomena, magnetic fields, and electric currents in active regions. I – Introduction and methods. *Astrophys. J.* **411**, 362. DOI. ADS.

Chintzoglou, G., Patsourakos, S., Vourlidas, A.: 2015, Formation of magnetic flux ropes during a confined flaring well before the onset of a pair of major coronal mass ejections. *Astrophys. J.* **809**, 34. DOI. ADS.

Dalmasse, K., Aulanier, G., Démoulin, P., Kliem, B., Török, T., Pariat, E.: 2015, The origin of net electric currents in solar active regions. *Astrophys. J.* **810**, 17. DOI. ADS.

Falconer, D.A.: 2001, A prospective method for predicting coronal mass ejections from vector magnetograms. *J. Geophys. Res.* **106**, 25185. DOI. ADS.

Falconer, D.A., Moore, R.L., Gary, G.A.: 2002, Correlation of the coronal mass ejection productivity of solar active regions with measures of their global nonpotentiality from vector magnetograms: baseline results. *Astrophys. J.* **569**, 1016. DOI. ADS.

Fletcher, L., Dennis, B.R., Hudson, H.S., Krucker, S., Phillips, K., Veronig, A., Battaglia, M., Bone, L., Caspi, A., Chen, Q., Gallagher, P., Grigis, P.T., Ji, H., Liu, W., Milligan, R.O., Temmer, M.: 2011, An observational overview of solar flares. *Space Sci. Rev.* **159**, 19. DOI. ADS.

Georgoulis, M.K.: 2012a, Are solar active regions with major flares more fractal, multifractal, or turbulent than others? *Solar Phys.* **276**, 161. DOI. ADS.

Georgoulis, M.K.: 2012b, On our ability to predict major solar flares. *Astrophys. Space Sci. Proc.* **30**, 93. DOI. ADS.

Georgoulis, M.K.: 2017, The ambivalent role of field-aligned electric currents in the solar atmosphere. In: Keiling, A., Marghitu, O., Wheatland, M. (eds.) *Electric Currents in Geospace and Beyond*, *AGU Monographs*.

Georgoulis, M.K., Rust, D.M.: 2007, Quantitative forecasting of major solar flares. *Astrophys. J. Lett.* **661**, L109. DOI. ADS.

Georgoulis, M.K., Titov, V.S., Mikić, Z.: 2012, Non-neutralized electric current patterns in solar active regions: origin of the shear-generating Lorentz force. *Astrophys. J.* **761**, 61. DOI. ADS.

Gosain, S., Démoulin, P., López Fuentes, M.: 2014, Distribution of electric currents in sunspots from photosphere to corona. *Astrophys. J.* **793**, 15. DOI. ADS.

Inoue, S., Hayashi, K., Magara, T., Choe, G.S., Park, Y.D.: 2015, Magnetohydrodynamic simulation of the X2.2 solar flare on 2011 February 15. II. Dynamics connecting the solar flare and the coronal mass ejection. *Astrophys. J.* **803**, 73. DOI. ADS.

Janvier, M., Aulanier, G., Bommier, V., Schmieder, B., Démoulin, P., Pariat, E.: 2014, Electric currents in flare ribbons: observations and three-dimensional standard model. *Astrophys. J.* **788**, 60. DOI. ADS.

Leka, K.D., Barnes, G.: 2003a, Photospheric magnetic field properties of flaring versus flare-quiet active regions. I. Data, general approach, and sample results. *Astrophys. J.* **595**, 1277. DOI. ADS.

Leka, K.D., Barnes, G.: 2003b, Photospheric magnetic field properties of flaring versus flare-quiet active regions. II. Discriminant analysis. *Astrophys. J.* **595**, 1296. DOI. ADS.

Leka, K.D., Barnes, G.: 2007, Photospheric magnetic field properties of flaring versus flare-quiet active regions. IV. A statistically significant sample. *Astrophys. J.* **656**, 1173. DOI. ADS.

Leka, K.D., Canfield, R.C., McClymont, A.N., van Driel-Gesztelyi, L.: 1996, Evidence for current-carrying emerging flux. *Astrophys. J.* **462**, 547. DOI. ADS.

McClymont, A.N., Jiao, L., Mikic, Z.: 1997, Problems and progress in computing three-dimensional coronal active region magnetic fields from boundary data. *Solar Phys.* **174**, 191. DOI. ADS.

Melrose, D.B.: 1991, Neutralized and unneutralized current patterns in the solar corona. *Astrophys. J.* **381**, 306. DOI. ADS.

Melrose, D.B.: 1995, Current paths in the corona and energy release in solar flares. *Astrophys. J.* **451**, 391. DOI. ADS.

Parker, E.N.: 1979, *Cosmical Magnetic Fields: Their Origin and Their Activity*. ADS.

Parker, E.N.: 1996, Inferring mean electric currents in unresolved fibril magnetic fields. *Astrophys. J.* **471**, 485. DOI. ADS.

Pesnell, W.D., Thompson, B.J., Chamberlin, P.C.: 2012, The Solar Dynamics Observatory (SDO). *Solar Phys.* **275**, 3. DOI. ADS.

Ravindra, B., Venkatakrishnan, P., Tiwari, S.K., Bhattacharyya, R.: 2011, Evolution of currents of opposite signs in the flare-productive solar active region NOAA 10930. *Astrophys. J.* **740**, 19. DOI. ADS.

Scherrer, P.H., Schou, J., Bush, R.I., Kosovichev, A.G., Bogart, R.S., Hoeksema, J.T., Liu, Y., Duvall, T.L., Zhao, J., Title, A.M., Schrijver, C.J., Tarbell, T.D., Tomczyk, S.: 2012, The Helioseismic and Magnetic Imager (HMI) investigation for the Solar Dynamics Observatory (SDO). *Solar Phys.* **275**, 207. DOI. ADS.

Schou, J., Scherrer, P.H., Bush, R.I., Wachter, R., Couvidat, S., Rabello-Soares, M.C., Bogart, R.S., Hoeksema, J.T., Liu, Y., Duvall, T.L., Akin, D.J., Allard, B.A., Miles, J.W., Rairden, R., Shine, R.A., Tarbell, T.D., Title, A.M., Wolfson, C.J., Elmore, D.F., Norton, A.A., Tomczyk, S.: 2012, Design and ground

calibration of the Helioseismic and Magnetic Imager (HMI) instrument on the Solar Dynamics Observatory (SDO). *Solar Phys.* **275**, 229. DOI. ADS.

Schrijver, C.J.: 2007, A characteristic magnetic field pattern associated with all major solar flares and its use in flare forecasting. *Astrophys. J. Lett.* **655**, L117. DOI. ADS.

Schrijver, C.J.: 2016, The nonpotentiality of coronae of solar active regions, the dynamics of the surface magnetic field, and the potential for large flares. *Astrophys. J.* **820**, 103. DOI. ADS.

Schrijver, C.J., DeRosa, M.L., Metcalf, T., Barnes, G., Lites, B., Tarbell, T., McTiernan, J., Valori, G., Wiegelmann, T., Wheatland, M.S., Amari, T., Aulanier, G., Démoulin, P., Fuhrmann, M., Kusano, K., Régnier, S., Thalmann, J.K.: 2008, Nonlinear force-free field modeling of a solar active region around the time of a major flare and coronal mass ejection. *Astrophys. J.* **675**, 1637. DOI. ADS.

Semel, M., Skumanich, A.: 1998, An ambiguity-free determination of J_Z in solar active regions. *Astron. Astrophys.* **331**, 383. ADS.

Shibata, K., Magara, T.: 2011, Solar flares: magnetohydrodynamic processes. *Living Rev. Solar Phys.* **8**, 6. DOI. ADS.

Syntelis, P., Gontikakis, C., Patsourakos, S., Tsinganos, K.: 2016, The spectroscopic imprint of the pre-eruptive configuration resulting into two major coronal mass ejections. *Astron. Astrophys.* **588**, A16. DOI. ADS.

Török, T., Leake, J.E., Titov, V.S., Archontis, V., Mikić, Z., Linton, M.G., Dalmasse, K., Aulanier, G., Kliem, B.: 2014, Distribution of electric currents in solar active regions. *Astrophys. J. Lett.* **782**, L10. DOI. ADS.

Vemareddy, P., Venkatakrishnan, P., Karthikreddy, S.: 2015, Flux emergence in the solar active region NOAA 11158: the evolution of net current. *Res. Astron. Astrophys.* **15**, 1547. DOI. ADS.

Wheatland, M.S.: 2000, Are electric currents in solar active regions neutralized? *Astrophys. J.* **532**, 616. DOI. ADS.

Wheatland, M.S.: 2005, Initial test of a Bayesian approach to solar flare prediction. *Publ. Astron. Soc. Aust.* **22**, 153. DOI. ADS.

Wilkinson, L.K., Emslie, A.G., Gary, G.A.: 1992, On neutralized currents in the solar corona. *Astrophys. J. Lett.* **392**, L39. DOI. ADS.

Yang, X., Zhang, H., Gao, Y., Guo, J., Lin, G.: 2012, A statistical study on photospheric magnetic nonpotentiality of active regions and its relationship with flares during Solar Cycles 22 – 23. *Solar Phys.* **280**, 165. DOI. ADS.

Zhang, H.: 1995, Formation of magnetic shear and an electric current system in an emerging flux region *Astron. Astrophys.* **304**, 541. ADS.